Postprint of: Sabik A., Kreja I., Thermo-elastic non-linear analysis of multilayered plates and shells, Composite Structures, Vol. 130, (2015), pp. 37-43, DOI: 10.1016/j.compstruct.2015.04.024

Sabik A.[*], Kreja I. [**]

Thermo-elastic non-linear analysis of multilayered plates and shells

Department of Structural Mechanics,
Gdańsk University of Technology, Narutowicza 11/12, 80-233 Gdańsk, Poland

*Corresponding author: e-mail: agsa@pg.gda.pl, phone: +48 58 347 21 74

**Corresponding author: e-mail: ikreja@pg.gda.pl, phone: +48 58 347 11 80

Abstract

Geometrically nonlinear FEM analysis of multilayered composite plates and shells is performed in order to resolve the stability problem of the structures being under the influence of temperature field. The Riks-Wempner-Ramm algorithm with a specially modified multi-choice unloading condition has been implemented in authors' numerical code. As the representation of multilayered medium the Equivalent Single Layer approach with the First Order Shear Deformation kinematics is employed. The effectiveness of the proposed model is examined in numerical examples with reference solutions available in the literature. Presented study proves that the proposed approach can be very effective in the analysis of stability of thin-walled thermally loaded panels.

Keywords: A. Layered Structures; B. Buckling; B. Thermomechanical; C. Computational modeling

1. Introduction

Multilayered structural materials like sandwich or composite laminates perfectly suit the demands for the application in thin-walled structures, which in natural manner are sensitive to instability effects. This paper concerns with the stability analysis of multilayered panels subjected to thermal loadings. The most popular approach in the analysis of structural instability is the linear analysis performed by solving a linearized eigenvalue problem. In this sense the buckling of thermally loaded composite plates and shells was considered within the framework of FEM modeling in [1, 2, 3, 4]. Matsunaga [5] examined the thermal buckling of laminated composites with power series expansion method. Approaches based on eigenvalue problem solution usually do not reveal the post-critical behavior, although Sita Thankam et al. [6] computed the post-critical temperatures by appropriate scaling of the first eigenmode. Nevertheless, such analyses are suitable only if the assumptions of linear work regime in the pre-buckling range are satisfied [7]. Otherwise, strategies taking into account the geometrically nonlinear effects must be employed, as an example the thermal or thermo-mechanical stability analyses of composite panels performed with the perturbation method by Shen [8, 9] or with the extended Galerkin method by Hause and Librescu [10, 11]. An interesting analytical approach was presented in [12], where the governing equations of the large deformation theory were handled with trigonometric power series expansion and the resulting nonlinear algebraic equations were solved by gradual step-by-step increase of thermal stresses to determine the unknown parameters. In [13] the non-linear differential equations are linearized and resolved by making use of Chebyshev polynomials.

There is a long record of successful applications of FEM analyses in the stability study of composite plates and shells. In contradiction to the analytical and semi-analytical approaches FEM does not impose any limitations as regard the geometry and boundary

conditions regularity, especially if more sophisticated shell theories are employed [14]. Except for the solving of the linearized eigenvalue problem the computations are often performed with static geometrically nonlinear incremental or dynamic explicit algorithms [15]. The explicit method is more robust in local buckling analyses [15], however, it does not control the equilibrium conditions, thus the user must take particular care of a proper choice of the analysis parameters.

In the present study, the static incremental analysis is performed. Such approach requires a proper path tracing method [16]. The load control strategy seems to be the simplest choice but it has a very limited applicability [17] in the stability analysis of thin-walled structures. The displacement control algorithms [18, 19] are more useful but they also fail when the turning point occurs on the equilibrium path for the selected control parameter. The arc-length control method is commonly recognized as the most effective technique for tracing complicated equilibrium paths. One should realize that due to various possible types of constraint equations there is a variety of arc-length control algorithms [20]. The arc-length methods are very powerful in tracing complicated equilibrium paths with various load limit or turning points, thus the post-critical paths can be determined without any major problems [21, 22, 23, 24, 25, 26]. However, to investigate the bifurcation instability, more sophisticated path tracing algorithms are necessary to determine the path direction in the arc-length methods (see e.g. papers by Feng et al. [27, 28, 29] for the case of mechanical loading and Parente et al. [24] for thermal influences). Very often such problems can be resolved in a simplified manner by imposing geometrical imperfections e.g. in the pattern of an eigenvalue mode, providing the tracing of an approximate secondary path [15, 27]. Nonetheless, such an approach is justified only for the cases with a linear response of the structure up to the bifurcation point. The fulfillment of this condition is strongly dependent i.a. on the material orthotropy determined by the material orientation in

subsequent layers [31]. Another way to trace the secondary paths is the application of additional small perturbation forces which are removed from the model after the solution quality change is detected, and the switching to the exact secondary path can be obtained in the subsequent unloading process [32]. In this paper, a similar method to the latter one is employed with such a difference that the loading process is continued after the elimination of the perturbation forces [25, 26]. It will be shown that such a tactic can be also very efficient.

2. Multilayered shell model

Among all possible approaches used in the modeling of multilayered media the most reasonable concept applicable in the analysis of entire shell structures is the Equivalent Single Layer (ESL) model [33, 34]. In such a concept which is employed in the present study the multilayered plate or shell is reduced to the two-dimensional reference surface with statically equivalent stiffness of the multilayered cross-section. It provides significant decrease of computational costs when compared with more advanced models like layer-wise or three-dimensional descriptions [33]. The transfer of the local equilibrium equations given in terms of continuum stress and strain measures to the cross-sectional level requires proper assumptions, very often imposed on the displacement unknowns. Due to a significant shear deformability of typical composite materials the models should take into account the transverse shear effect. Depending on the polynomial degree used in the description of the displacement distribution in the thickness direction one can distinguish the group of the First Order Shear Deformation (FOSD) and the group of Higher Order Shear Deformation (HOSD) models. Although in all of the FOSD models the transverse deformation profile is described by a linear function, the authors talk intentionally about the group of these models, since various variants of typical for these approaches shear correction methods can be adopted [35,

36]. It can be shown, that the usage of FOSD theory with a proper shear correction technique leads to very good results [37]. Due to their earlier positive experience the authors employ the FOSD model in the present study on thermally loaded plates and shells.

2.1 *Shell kinematics*

The detailed description of the assumed shell kinematics can be found in [25, 26]. Therefore, only the final formulas are presented in this paper. The Greek indices are equal to 1 or 2, whereas the Latin ones are 1, 2 or 3. The curvilinear coordinates of the shell $\theta^1,\theta^2,\theta^3$ are implemented with θ^1,θ^2 being the mid-surface coordinates and θ^3 standing for the transverse normal coordinate. Moreover, the left superscript indicates the configuration in which the value is obtained, while the left subscript describes the configuration the value refers to. Precisely the superscript *m* and subscripts arising in the following mean: the actual configuration (*m*=*t*=1), the unknown configuration (*m*=*t*=2) and the reference configuration (*t*=*m*=0), since the Total Lagrangian description is employed.

Due to the presumed inextensibility of the fiber in the transverse normal direction the displacement field is described by 5 independent parameters:

$$ {}^{m}\upsilon_{\alpha}(\theta^1,\theta^2,\theta^3) = {}^{m}\overset{(0)}{\upsilon}_{\alpha}(\theta^1,\theta^2) + \theta^3\, {}^{m}\overset{(1)}{\upsilon}_{\alpha}(\theta^1,\theta^2), \qquad {}^{m}\upsilon_{3}(\theta^1,\theta^2,\theta^3) = {}^{m}\overset{(0)}{\upsilon}_{3}(\theta^1,\theta^2) = const. \tag{1} $$

The bending strains at any point of the shell are related to the two-dimensional strain measures as follows:

$$ {}^{m}_{0}E_{\alpha\beta}(\theta^1,\theta^2,\theta^3) = {}^{m}_{0}\overset{(0)}{E}_{\alpha\beta}(\theta^1,\theta^2) + \theta^3\, {}^{m}_{0}\overset{(1)}{E}_{\alpha\beta}(\theta^1,\theta^2) + \left(\theta^3\right)^2 {}^{m}_{0}\overset{(2)}{E}_{\alpha\beta}(\theta^1,\theta^2), \tag{2} $$

where the two-dimensional strain measures are obtained from the following strain-displacement relations

$$
\begin{aligned}
2\,{}^{m}_{0}E^{(0)}_{\alpha\beta} &= {}^{m}\varphi^{(0)}_{\beta\alpha} + {}^{m}\varphi^{(0)}_{\alpha\beta} + {}^{m}\varphi^{(0)}_{\delta\alpha}\,{}^{m}\varphi^{(0)\delta}_{\beta} + {}^{m}\varphi^{(0)}_{\alpha 3}\,{}^{m}\varphi^{(0)}_{\beta 3},\\
2\,{}^{m}_{0}E^{(1)}_{\alpha\beta} &= {}^{m}\upsilon^{(1)}_{\beta}\big|_{\alpha} + {}^{m}\upsilon^{(1)}_{\alpha}\big|_{\beta} - {}^{0}b^{\lambda}_{\alpha}\,{}^{m}\varphi^{(0)}_{\lambda\beta} - {}^{0}b^{\lambda}_{\beta}\,{}^{m}\varphi^{(0)}_{\lambda\alpha} + {}^{m}\upsilon^{(1)}_{\delta}\big|_{\alpha}\,{}^{m}\varphi^{(0)\delta}_{\beta} + {}^{m}\upsilon^{(1)}_{\delta}\big|_{\beta}\,{}^{m}\varphi^{(0)\delta}_{\alpha} +\\
&\quad + {}^{m}\varphi^{(0)}_{\beta 3}\,{}^{m}\upsilon^{(1)}_{\lambda}\,{}^{0}b^{\lambda}_{\alpha} + {}^{m}\varphi^{(0)}_{\alpha 3}\,{}^{m}\upsilon^{(1)}_{\lambda}\,{}^{0}b^{\lambda}_{\beta},\\
2\,{}^{m}_{0}E^{(2)}_{\alpha\beta} &= -{}^{0}b^{\lambda}_{\alpha}\,{}^{m}\upsilon^{(1)}_{\lambda}\big|_{\beta} - {}^{0}b^{\delta}_{\beta}\,{}^{m}\upsilon^{(1)}_{\delta}\big|_{\alpha} + {}^{m}\upsilon^{(1)\lambda}\big|_{\alpha}\,{}^{m}\upsilon^{(1)}_{\lambda}\big|_{\beta} + \left({}^{m}\upsilon^{(1)}_{\delta}\,{}^{0}b^{\delta}_{\alpha}\right)\left({}^{m}\upsilon^{(1)}_{\lambda}\,{}^{0}b^{\lambda}_{\beta}\right).
\end{aligned}
\tag{3}
$$

The analogously relations valid for the transverse shear can be written as:

$$
{}^{m}_{0}E_{\alpha 3}(\theta^1,\theta^2,\theta^3) = {}^{m}_{0}E^{(0)}_{\alpha 3}(\theta^1,\theta^2),
\tag{4}
$$

where the two-dimensional strain measures result from:

$$
2\,{}^{m}_{0}E^{(0)}_{\alpha 3} = {}^{m}\upsilon^{(1)}_{\alpha} + {}^{m}\varphi^{(0)}_{\alpha 3} + {}^{m}\varphi^{(0)\lambda}_{\alpha}\,{}^{m}\upsilon^{(1)}_{\lambda}\,.
\tag{5}
$$

The r.h.s. terms in (3) and (5) are obtained from:

$$
\begin{aligned}
&{}^{m}\varphi^{(0)}_{\alpha\beta} = {}^{m}\upsilon^{(0)}_{\alpha}\big|_{\beta} - {}^{m}\upsilon^{(0)}_{3}\,{}^{0}b_{\alpha\beta}, \qquad {}^{m}\varphi^{(0)}_{\alpha 3} = {}^{m}\upsilon^{(0)}_{\lambda}\,{}^{0}b^{\lambda}_{\alpha} + {}^{m}\upsilon^{(0)}_{3},_{\alpha}, \qquad {}^{m}\varphi^{(0)\delta}_{\beta} = {}^{m}\upsilon^{(0)\delta}\big|_{\beta} - {}^{m}\upsilon^{(0)}_{3}\,{}^{0}b^{\delta}_{\beta},\\
&{}^{m}\varphi^{(1)}_{\alpha\beta} = {}^{m}\upsilon^{(1)}_{\alpha}\big|_{\beta}, \qquad\qquad {}^{m}\varphi^{(1)}_{\alpha 3} = {}^{m}\upsilon^{(1)}_{\lambda}\,{}^{0}b^{\lambda}_{\alpha}, \qquad\qquad {}^{m}\varphi^{(1)\delta}_{\beta} = {}^{m}\upsilon^{(1)\delta}\big|_{\beta}.
\end{aligned}
\tag{6}
$$

The vertical lines in (3) and (6) stand for the covariant differentiation of displacement vector components.

2.2 *Governing equations*

In the state of equilibrium the balance between the internal and external virtual works is satisfied:

$$
{}^{2}\delta W_i = {}^{2}\delta W_e, \qquad {}^{2}\delta W_i = \int_{{}^{0}V}\left(\left({}^{1}_{0}S^{mn}_{mech} + {}_{0}S^{mn}_{mech}\right) - {}^{2}_{0}S^{mn}_{th}\right)\delta_{0}E_{mn}\,{}^{0}dV
\tag{7}
$$

Since the mechanical loads are not considered in the present study, the external work term in (7) is equal to zero. The internal work is expressed in terms of strain and stress measures valid for the Total Lagrangian description. The $\delta_{0}E_{mn}$ is the variation of the components of the Green-Lagrange strain tensor, ${}^{1}_{0}S^{mn}_{mech}$ are the mechanical stresses accumulated during the incremental process, ${}_{0}S^{mn}_{mech}$ stands for the increment of the mechanical stresses and ${}^{2}_{0}S^{mn}_{th}$ are the thermal stresses in the unknown configuration.

After the pre-integration in the thickness direction in (7) we can calculate the increment of mechanical resultant forces:

$$\left\{ {}_0\mathcal{S}_{mech} \right\} = \left[{}_0\mathcal{H}_{mech} \right] \left\{ {}_0\mathcal{E}_{mech} \right\} \quad \Leftrightarrow \quad \begin{Bmatrix} \left\{ {}_0\mathcal{N}_{mech} \right\} \\ \left\{ {}_0\mathcal{M}_{mech} \right\} \\ \left\{ {}_0\mathcal{B}_{mech} \right\} \\ \left\{ {}_0\mathcal{Q}_{mech} \right\} \end{Bmatrix} = \begin{bmatrix} \overset{(0,0)}{[A]_{3\times3}} & \overset{(0,1)}{[B]_{3\times3}} & \overset{(0,2)}{[D]_{3\times3}} & [0]_{3\times2} \\ \overset{(1,0)}{[B]_{3\times3}} & \overset{(1,1)}{[D]_{3\times3}} & \overset{(1,2)}{[E]_{3\times3}} & [0]_{3\times2} \\ \overset{(2,0)}{[D]_{3\times3}} & \overset{(2,1)}{[E]_{3\times3}} & \overset{(2,2)}{[F]_{3\times3}} & [0]_{3\times2} \\ [0]_{2\times3} & [0]_{2\times3} & [0]_{2\times3} & \overset{(0,0)}{[S_A]_{2\times2}} \end{bmatrix} \begin{Bmatrix} \left\{ {}_0\varepsilon^{(0)} \right\} \\ \left\{ {}_0\varepsilon^{(1)} \right\} \\ \left\{ {}_0\varepsilon^{(2)} \right\} \\ \left\{ {}_0\gamma^{(0)} \right\} \end{Bmatrix}, \tag{8}$$

and the resultant thermal forces:

$$\left\{ {}^2_0\mathcal{S}_{th} \right\} = \left[{}_0\mathcal{H}_{th} \right] \left\{ {}^2_0\mathcal{T} \right\} \quad \Leftrightarrow \quad \begin{Bmatrix} \left\{ {}^2_0\mathcal{N}_{th} \right\} \\ \left\{ {}^2_0\mathcal{M}_{th} \right\} \\ \left\{ {}^2_0\mathcal{B}_{th} \right\} \\ \{ 0 \} \end{Bmatrix} = \begin{bmatrix} \overset{(0,0)}{\{A_{th}\}_{3\times1}} & \overset{(0,1)}{\{B_{th}\}_{3\times1}} \\ \overset{(1,0)}{\{B_{th}\}_{3\times1}} & \overset{(1,1)}{\{D_{th}\}_{3\times1}} \\ \overset{(2,0)}{\{D_{th}\}_{3\times1}} & \overset{(2,1)}{\{E_{th}\}_{3\times1}} \\ \{0\}_{2\times1} & \{0\}_{2\times1} \end{bmatrix} \begin{Bmatrix} T^{(0)} \\ T^{(1)} \end{Bmatrix}. \tag{9}$$

The components of the strain sub-vectors on the r.h.s. in (8) are the 2-dimensional strain measures as displayed in equation (2) and (4), whereas the temperatures $T^{(0)}$ and $T^{(1)}$ in (9) are the measures of the uniform heating and thermal gradient, respectively [26].

The components of the sub-matrices of the constitutive matrix $\left[{}_0\mathcal{H}_{mech} \right]$ in (8) are calculated as follows:

$$\begin{aligned} \left[A_{ij},\ B_{ij},\ D_{ij},\ E_{ij},\ F_{ij} \right] &= c_{ij} \int_{-\frac{H}{2}}^{\frac{H}{2}} \left[1,\ \theta^3,\ \left(\theta^3\right)^2,\ \left(\theta^3\right)^3,\ \left(\theta^3\right)^4 \right] {}^0\mu d\theta^3, \quad i, j = 1,2,3 \\ \left[S_{Aij} \right] &= \int_{-\frac{H}{2}}^{\frac{H}{2}} c_{ij}\ {}^0\mu d\theta^3, \quad i, j = 4,5 \end{aligned} \tag{10}$$

where c_{ij} are the elements of the layer constitutive matrix defined for the transversely isotropic material transferred into the global coordinate system θ^1-θ^2-θ^3 [26]. The ${}^o\mu$ term is the determinant of the shifter tensor [25, 26]. The components of the sub-matrix need to be corrected by the shear correction factors k_{13} and k_{23} [25, 26]. They are

evaluated numerically, separately for each transverse shear plane, following the concept proposed by Whitney [35] and extended later on by Figueiras and Owen [36]. Similarly, the elements of constitutive sub-vectors $\left[{}_0\mathcal{H}_{th} \right]$ in (9) result from the following formulas:

$$\left[A_{th}^i, \quad B_{th}^i, \quad D_{th}^i, \quad E_{th}^i \right] = c_{th}^i \int_{-\frac{h}{2}}^{\frac{h}{2}} \left[1, \quad \theta^3, \quad \left(\theta^3\right)^2, \quad \left(\theta^3\right)^3 \right] \theta^{3\,0} \mu d\theta^3, \quad i = 1,2,3 \tag{11}$$

where c_{th}^i are the components of the thermal constitutive vectors of each material in the stacking sequence of layers transferred to the global system θ^1-θ^2-θ^3 [26].

3. Path tracing method

The incremental equation which is to be solved has a form:

$$\mathsf{K}\left({}^1\mathsf{q}, {}^2\lambda_{th}, \Delta T_{REF}\right)\Delta\mathsf{q} = {}^2\lambda_{th}\mathsf{F}_{th}\left({}^1\mathsf{q}, \Delta T_{REF}\right) - \mathsf{F}\left({}^1\mathsf{q}\right), \tag{12}$$

where K, F_{th} and F are the global tangent stiffness matrix, thermal load vector and balanced force vector, respectively. All the terms are dependent on the actual displacement ${}^1\mathsf{q}$ and in addition, K and F_{th} are concurrently functions of the temperature in the unknown configuration, since $\Delta T_{REF} = T_{max} - T_{init}$ is the total temperature applied to the structure on the leading surface [26] and ${}^2\lambda_{th}$ is the load parameter in the unknown configuration (t=2). To trace the equilibrium path of the structure, the Riks-Wempner-Ramm (RWR) algorithm [38] is adopted. The increment and iteration numbers are distinguished with the use of two superscripts, whereas the left one stands for the increment number (n) and the right one signifies the number of the iteration (i). In each step of the analysis the following equation of spherical arc-length control method must be satisfied:

$$\left({}^n\Delta\mathsf{q}^{(0)}\right)^T\left({}^n\Delta\mathsf{q}^{(0)}\right) + \left({}^n\Delta\lambda_{th}^{(0)}\right)^2 = {}^n ds^2, \tag{13}$$

where *ds* is the arc-length parameter. During the iteration process the solution is corrected according to:

$$
\begin{aligned}
{}^{n}\mathsf{q}^{(i)} &= {}^{n}\mathsf{q}^{(i-1)} + {}^{n}\delta\mathsf{q}^{(i)}, \\
{}^{n}\lambda_{th}^{(i)} &= {}^{n}\lambda_{th}^{(i-1)} + {}^{n}\delta\lambda_{th}^{(i)}.
\end{aligned}
\tag{14}
$$

The corrections ${}^{n}\delta\mathsf{q}^{(i)}$ and ${}^{n}\delta\lambda_{th}^{(i)}$ in the RWR algorithm are searched in the tangential direction to the preceding approximation:

$$
\left({}^{n}\Delta\mathsf{q}^{(i-1)}\right)^{T}\left({}^{n}\delta\mathsf{q}^{(i)}\right) + {}^{n}\Delta\lambda_{th}^{(i-1)}\,{}^{n}\delta\lambda_{th}^{(i)} = 0\,. \tag{15}
$$

One has to stress that at the beginning of each incremental step the sign of the initial load parameter increment has to be determined. Therefore, the equation (13) has to be supplemented by an additional unloading condition. In the present study two conditions are implemented. The first one, signified as ICRIT=0, states, that the sign of the load parameter increment is equal to the sign of the global stiffness matrix determinant, i.e.:

$$
\operatorname{sgn}\left({}^{n}\Delta\lambda_{th}^{(0)}\right) = \operatorname{sgn}\left|\mathsf{K}\left({}^{(n-1)}\mathsf{q},\,{}^{(n-1)}\lambda_{th},\,\Delta T_{REF}\right)\right| \tag{16}
$$

The second one, indicated as ICRIT=1, assumes that the direction in which the new step should proceed is determined by the direction obtained in the previous step [26]. The final formula for a sign of the load parameter increment has a form:

$$
\operatorname{sgn}\left({}^{n}\Delta\lambda_{th}^{(0)}\right) = \operatorname{sgn}\left(\left({}^{(n-1)}\Delta\mathsf{q}\right)^{T}\left({}^{n}\Delta\mathsf{q}_{REF}\right) + {}^{(n-1)}\Delta\lambda_{th}\right), \tag{17}
$$

with ${}^{n}\Delta\mathsf{q}_{REF}$ calculated in step *n* for to the total applied temperature [26].

4. Numerical examples

To show the efficiency of the proposed formulation several numerical examples are considered. The FE discretization was performed with the isoparametric doubly curved Serendipity type 8-node shell elements utilizing the uniformly reduced integration technique (8URI) [25, 26, 39]. If appropriate strength data are available, an additional

study of failure initiation is made in accordance with the Tsai-Wu criterion, whereas stresses are obtained at the Gauss points matching the 2x2scheme of integration.

4.1 *Sandwich plate*

This example was originally proposed in [40] and later on it was analyzed in [2]. The buckling temperature of a uniformly heated quadratic (A=B) sandwich plate with aspect ratio A/H=20 is considered (Fig. 1a). The angle α in Figure 1 determines the fibers reinforcement direction. All four edges are simply supported with the translations fixed in three directions. The outer faces of the plate are made of a laminate and the core is composed of the honeycomb structure. The parameterized material data of the laminate are: E_a/E_{b*}=19, G_{ab}/E_{b*}=0.52, G_{bc}/E_{b*}=0.338, ν_{ab}=0.32, $\alpha_{aa}^{th}/\alpha_0^{th}$=0.001, $\alpha_{bb}^{th}/\alpha_0^{th}$=1, where a and b denote the fiber direction and the direction perpendicular to the fiber, respectively. The core material data are determined as follows: $E_a/E_{b*}=3.2\cdot10^{-5}$, $E_b/E_{b*}=2.9\cdot10^{-5}$, $G_{ab}/E_{b*}=2.4\cdot10^{-3}$, $G_{ac}/E_{b*}=7.9\cdot10^{-2}$, $G_{bc}/E_{b*}=6.6\cdot10^{-2}$, ν_{ab}=0.99, $\alpha_{aa}^{th}/\alpha_0^{th}=\alpha_{bb}^{th}/\alpha_0^{th}$=1.36. The coefficient α_0^{th} is the normalization measure of the thermal expansion coefficient and E_{b*} is the Young's module of the faces' material in the direction perpendicular to the reinforcement. The stacking sequence of the sandwich layers is following ($[0^\circ/90^\circ]_5$, core, $[90^\circ/0^\circ]_5$).

Due to the symmetry conditions the structure bifurcates at a specific critical temperature. The attractiveness of this particular example consists in an existence of the three-dimensional reference solution [40]. The normalized results are presented in a form of the coefficient λ_T, whereas $\lambda_T=\alpha_0^{th}T_{\mathrm{cr}}$. Assuming that H_o symbolizes the thickness of a single face, H is the total sandwich thickness and $m=H_o/H$, 5 laminations are studied, described by m equal to 0.025, 0.05, 0.075, 0.1, or 0.15. The mesh of 10x10 8URI elements was used in the analysis. The uniform heating was modeled as a very small thermal gradient, i.e. of the rank $T_{\mathrm{bottom}}/T_{\mathrm{top}}$=0.999999, in order to obtain the

critical temperatures. In such a case the choice of the unloading condition is irrelevant. The graphs in Figure 2 display the comparison of the present results with the 3D solution given by Noor et al. [40] (3D) and the 2-dimensional ones obtained in [2] with the use of FOSD and HOSD models. The results obtained with the HOSD model are in very good agreement with the 3D solution [40]. In the contrary, the critical temperatures resulting from FOSD model [2] tend to disagree with the Noor's solution as the parameter *m* increases. One can suppose that this is due to the inappropriate values of the shear correction factors employed in [2] (k=5/6). Therefore, in the present study two analyses were made: with the use of the imposed value k=5/6 (present k13=k23=5/6) and the values obtained numerically (present k13<>k23). It can be seen that the usage of shear factors given not a priori leads to solutions which are close to the 3D ones; nevertheless, the results from the computations performed with k=5/6 agree with that obtained with the FOSD model [2]. This confirms that the present model with shear correction factors evaluated numerically can be competitive to the HOSD model.

4.2 *Cylindrical cross-ply shell*

A cylindrical cross-ply $[0^\circ/90^\circ]_s$ shell under uniform temperature rise, as proposed in [22, 23], is considered. The geometry of the panel is defined by $A=B=R\phi$, $\phi=15^\circ$, A/H=200 (Fig.1b). The edges of the shell are simply supported being not free to translate in any direction. The layers are made of material with the following data: E_a=138GPa, E_b=8.28GPa, $G_{ab}=G_{ac}=G_{bc}$=6.9GPa, ν_{ab}=0.33, $\alpha_{aa}^{th}=0.18\cdot10^{-6}$1/°C, $\alpha_{bb}^{th}=27\cdot10^{-6}$1/°C, $X_t=X_c$=1263MPa, Y_t=33.7MPa, Y_c=207MPa, S_s=57.3MPa, where X_t, X_c are the tensile and compressive strength in the direction a, Y_t, Y_c are the analogical parameters in the direction b, and S_s is the shear strength in the layer plane. In the present analysis, the mesh of 10x10 8URI elements was adopted. Figure 3a depicts the comparison of the reference solution with the present results obtained with the use of

two different unloading conditions. By selecting ICRIT=1 the whole path in the range of analyzed temperatures can be found. The discrepancies between the present and reference results [22, 23] can be caused by a different type of composite modeling in these two approaches. In the opposite, if ICRIT=0, severe convergence problems arise at about 260˚C, suggesting an existence of a bifurcation point in a vicinity. To find the post-critical path the additional study was performed with small perturbation forces, which were removed from the model after the quality change of the solution as compared with the primary path was detected. The magnitudes of the applied forces were of the level corresponding to deflections not bigger than 0.001*H*. Since the location of the imperfection forces was not obvious it was determined by a trial and an error method. The chosen points and the obtained results are depicted in Figure 3a and 3b. The force located at point E on the symmetry axis along the height of the panel did not change the solution. However, all other forces, applied separately or simultaneously, caused the solution conversion to the same post-critical path (imp A, B, C, D and A-D). One has also to stress that the perturbation force located at point D, i.e. on the other side of the symmetry axis than the other forces, causes the deformation which is the mirror pattern of the deformation induced by forces at points A, B, C or all forces applied simultaneously (Figure 3b). The detected bifurcation point is symmetrical and unstable what is clearly demonstrated on the basis of the circumferential translation of the central point of the shell (Figure 3b). Finally, it is worth mentioning that the strength analysis performed according to the Tsai-Wu hypothesis showed no failure in the range of studied temperatures.

4.3 *Cylindrical angle-ply shell*

A cylindrical angle-ply composite shell under uniform temperature rise as proposed in [21] is analyzed. The following geometric data are assumed: $A=B=R\phi$, R/A=5, A/H=200 (Figure 1b). All four edges of the panel are fixed against the translations in

three directions and rotations about the normal lines to the edges. The material properties of layers are the same as in the example 4.2. The fibers orientation varies in the stacking sequence according to an acute angle 67.5˚, i.e. [67.5˚/-67.5˚/…]. The influence of the number of layers N is studied, whereas N takes the values N=2, 4 and 8. The present study shows that the successive doubling of N value above N=8 does not change the solution and therefore this value can be treated as an infinite one (N=8=∞). The mesh of 12x12 8URI elements was used in the analysis. During the incremental process the unloading condition ICRIT=1 was employed. For the sake of the failure initiation examination, the top and bottom layers were divided into two sub-layers, while the outer ones had the thickness 0.01H. One has to stress here, that in [21] the location of stress control points is not described in details.

One can deduce that the reference solutions [21] were obtained by taking advantage of symmetry conditions. In the case of the shells made of 2 and 4 layers a half of the panel was studied, whereas only a quarter of the structure was analyzed in the case of N=8=∞. In the present study, however, the whole panels were considered in order not to impose only symmetrical deformation patterns. Moreover, one has to notice that the considered angle-ply lamination scheme which is unsymmetrical with the reference to the shell mid-plane disturbs the symmetry of the problem. The comparison of the present results with the reference solutions [21] is illustrated in Figure 4. A very good agreement is observed for N=2 and N=4. However, significant quality discrepancies are detected in the case of a shell composed of 8 layers, if series ‘N=8’ and ‘Huang N=inf. (1/4)’ are compared. Therefore, an additional analysis was performed with the use of double symmetry conditions. The obtained series is marked as N=8 (1/4) in Figure 4. It is comparable with the reference solution obtained by Huang et al. [21]. This proves that the use of biaxial symmetry conditions in this example is evidently incorrect. The strength analysis indicates that the failure arise in the bottom layers at temperatures

T_{TW}=247˚C, T_{TW}=282˚C and T_{TW}=288˚C for N=2, 4 and N=8=∞, respectively. In [21] the following failure temperatures resulting from the Tsai-Wu theory for each number of layers are reported: T_{TW}=255˚C, T_{TW}=250˚C, T_{TW}=230˚C. The observed disagreements can be caused by various reasons like other finite element types and a different distribution of stress recovery points as discussed in [26]. In the case of shell with N=8=∞ the disagreement results obviously from the symmetry conditions imposed in [21]. This supposition can be partially supported by the fact, that in the present analysis of a quarter of the panel the detected failure temperature has a value T_{TW}=222˚C, which is comparable with the reference one [21].

4.4 *Spherical cross-ply shell*

This example is taken after [21]. A spherical shell under uniform temperature distribution is considered. The following geometrical data are assumed: A=B, R/A=10, A/H=100 (Figure 1c). All four edges are fixed against three translations and the rotations about the normal lines. The panel is un-symmetrically laminated, i.e. [0˚/90˚/0˚/90˚], and the layers are made of the material with the following parameters: E_a=76GPa, E_b=5.5GPa, G_{ab}=G_{ac}=2.3GPa, G_{bc}=1.5GPa, v_{ab}=0.34, α_{aa}^{th}=-4·10^{-6}1/˚C, α_{bb}^{th}=79·10^{-6}1/˚C, X_t=1400GPa, X_c=235MPa, Y_t=12MPa, Y_c=53MPa, S_s=34MPa.

In the present analysis, the whole panel was modeled with the mesh of 12x12 8URI elements. Figure 5 illustrates the comparison between the present and reference results [21], which are very close to each other. The behavior of the shell is stable in the considered range of temperatures. The further load increase was not continued in [21], probably because of the material failure taking place at T_{TW}=121˚C.

The additional parametric study was performed in order to check the influence of the fibers arrangement in the sequence of layers and the following schemes were adopted: [45˚/-45˚/45˚/-45˚], [30˚/-30˚/30˚/-30˚], [15˚/-15˚/15˚/-15˚], [0˚/0˚/0˚/0˚]. The

results are presented in Figure 5. The fibers arrangement influences the stability behavior of the shell in a significant manner. With the decrease of the angle α the behavior of the structure becomes explicitly non-linear and if α is small, the shell undergoes a snap-through instability (Figure 5). In all cases besides the orthotropic one [0˚/0˚/0˚/0˚] the selection of the unloading condition is irrelevant. However, the use of ICRIT=0 in the analysis of the orthotropic shell leads to oscillatory problems, as shown in Figure 5. To detect a possible bifurcation point and a secondary path additional study with small perturbation forces was carried out but no other solution was obtained than the primary path. Presumably, the tracing of secondary path is in this case hampered due to a possible very close proximity of bifurcation and load limit points. The strength study was made in the middle of each layer's thicknesses. Table 1 includes the obtained failure temperatures and failure location. The material of shells [15˚/-15˚/15˚/-15˚] and [0˚/0˚/0˚/0˚] starts to fail after the passing of load limit point. In [21] the failure temperature obtained for [0˚/90˚/0˚/90˚] lay-up according to the Tsai-Wu theory was T_{TW}=115˚C, which is close to that obtained in the present study. Comparison of the results achieved in the analyses of [0˚/90˚/0˚/90˚] and [45˚/-45˚/45˚/-45˚] shells suggests that the behavior of these panels is the same. One has however to stress that the deformation of the cross-ply shell is bisymmetrical, whereas in the case the angle-ply lay-up [45˚/-45˚/45˚/-45˚] a skew symmetry of deformation pattern is observed [25].

Table 1. Failure temperatures and failure locations of considered spherical shells

Layers arrangement	Failure temperature	Failure location
[0˚/90˚/0˚/90˚]	121˚C	Bottom layer
[45˚/-45˚/45˚/-45˚]	123˚C	Bottom layer
[30˚/-30˚/30˚/-30˚]	102˚C	Top layer
[15˚/-15˚/15˚/-15˚]	44˚C	Bottom layer
[0˚/0˚/0˚/0˚]	36˚C	Bottom layer

5. Conclusions

An effectiveness study of the proposed FEM model for multilayered composite plates and shells under the temperature influence was presented. The multilayered shell body was considered as an equivalent single layer with the average resultant stiffness of the multilayered cross-section, whereas the first order shear deformation theory kinematic assumptions were taken into account. The authors focused on the thermal stability problem which was analyzed on the basis of the geometrically non-linear incremental approach. In the analysis the authors' own numerical code was employed. Special attention was paid to the proper path tracing method. It was shown that the most powerful technique, namely the arc-length method, required a proper unloading condition deciding whether the load should increase or decrease. The specially proposed multi-choice condition enabled to find primary paths if the previously obtained direction was followed (ICRIT=1) or to detect the bifurcation points if the sign of the stiffness matrix determinant was controlled (ICRIT=0). Moreover, the secondary paths were also traced in the study by employing load imperfections. The adopted conditions itself are widely described in the literature [24, 27, 28, 29], being examined there in the analysis of isotropic structures only. This work extends their application onto the analysis of multilayered media. Admittedly, Lee et al. [22] and Oh et al. [23] adopted also a similar approach as (ICRIT=1) in the cylindrical arc-length method to trace the equilibrium paths of multilayered shells, but they did not investigate the bifurcation points and secondary paths as it was done in the present study. In the authors' opinion the multi-choice formulation of the unloading condition provides a more detailed stability analysis than the single condition application itself. One has also to stress, that in the presented approach the primary paths can be followed without utilizing of any simplifications as for example symmetry conditions, which, as

it was shown, should be used with a particular care in the analysis of multilayered media.

Additionally, a simultaneously failure initiation analysis was carried out according to the Tsai-Wu hypothesis. The strength analysis had a passive character, i.e. the stiffness parameters remained constant regardless the eventually detected failure. Moreover, the temperature dependency of material parameters was in the model ignored. On the basis of the representative numerical examples it was shown that the stability problems were very essential in the load capacity analysis of thin panels and that the proposed path tracing algorithm was very effective. The authors hope to extend the presented model in further investigations taking into account the thermal degradation of material parameters and stiffness reduction according to the detected failure mechanisms.

ACKNOWLEDGEMENTS

The first author acknowledges financial support from the National Centre for Research and Development of Poland under grant “Fobridge”, PBS1/B2/6/2013.

REFERENCES

1. Lee J. Thermally induced buckling of laminated composites by a layerwise theory. Comput Struct 1997;65:917-922.
2. Kant T, Babu CS. Thermal buckling analysis of skew fibre-reinforced composite and sandwich plates using shear deformable finite element models. Compos Struct 2000;49:77-85.
3. Kabir HRH, Askar H, Chaudhuri RA. Thermal buckling response of shear flexible laminated anisotropic plates using a three-node isoparametric element. Compos Struct 2003;59:173-187.
4. Lal A, Singh BN, Kale S. Stochastic post buckling analysis of laminated composite cylindrical shell panel subjected to hygrothermomechanical loading. Compos Struct 2011;93:1187-1200.
5. Matsunaga H. Thermal buckling of cross-ply laminated composite shallow shells according to a global higher-order deformation theory. Compos Struct 2007;81:210-221.
6. Sita Thankam V, Singh G, Venkateswara R, Rath AK. Thermal post-buckling behaviour of laminated plates using a shear-flexible element based on couple-displacement field. Compos Struct 2003;59:351-359.
7. Koiter WT. Discussion “The Linearization of the Prebuckling State and Its Effect on the Determined Instability Loads” (by Kerr AD, Soifer MT. ASME J. Appl. Mech 1969;36:775–783) ASME J. Appl. Mech 1970;37:882-883.
8. Shen HS, Lin ZQ. Thermal post-buckling analysis of imperfect laminated plates. Comput Struct 1995;57:533-540.
9. Shen HS. Thermal postbuckling behavior of imperfect shear deformable laminated plates with temperature-dependent properties. Comput Method Appl M 2001;190:5377-5390.
10. Hause T, Librescu T. Non-linear response of geometrically imperfect sandwich curved panels under thermomechanical loading. Int J Nonlinear Mech 1998;33:1039-1059.
11. Librescu L, Hause T. Recent developments in the modeling and behavior of advanced sandwich constructions: a survey. Compos Struct 2000;48:1-17.
12. Zakeri AA, Alinia MM. An analytical study on post-buckling behaviour of imperfect sandwich panels subjected to uniform thermal stresses. Thin Wall Struct 2006;44:344-353.

13. Shukla KK, Nath Y. Analytical solution for buckling and post-buckling of angle-ply laminated plates under thermomechanical loading. Int J Nonlinear Mech 2001;36:1097-1108.
14. Chróścielewski J, Kreja I, Sabik A, Witkowski W. Modeling of composite shells in 6–parameter nonlinear theory with drilling degree of freedom. Mech Adv Mat Struct 2011;18:403-419.
15. Kobayashi T, Mihara Y, Fujii F. Path-tracing analysis for post-buckling process of elastic cylindrical shells under axial compression. Thin Wall Struct 2012;61:180-187.
16. Waszczyszyn Z. Numerical problems of nonlinear stability analysis of elastic structures. Comput Struct 1983;17:13-24.
17. Kundu CK, Han JH. Nonlinear buckling analysis of hygrothermoelastic composite shell panels using finite element metod. Compos Part B 2009;40:313-328.
18. Joshi RM, Patel BP. Nonlinear thermoelastic response of laminated conical panels. Struct Eng Mech 2010;34:97-107.
19. Marcinowski J. Large deflections of shells subjected to an external load and temperature changes. Int J Solids Struct 1997;34:755-768.
20. Carrera E. A study on arc-length-type methods and their operation failures illustrated by a simple model. Comput Struct 1994;50:217-229.
21. Huang NN, Tauchert TR. Large deflections of laminated cylindrical and doubly-curved panels under thermal loading. Comput Struct 1991;41:303-312.
22. Lee JJ, Oh IK, Lee I, Yeom CH. Thermal post-buckling behavior of patched laminated panels under uniform and non-uniform temperature distributions. Compos Struct 2002;55:137-145.
23. Oh IK, Lee I. Thermal snapping and vibration characteristics of cylindrical composite panels using layerwise theory. Compos Struct 2001;51:49-61.
24. Parente EJr, de Holanda AS, Afonso da Silva SMB. Tracing nonlinear equilibrium paths of structures subjected to thermal loading. Comput Mech 2006;38:505-520.
25. Sabik A. Stability analysis of thermally loaded multilayered shells (in Polish). Monographs of Gdansk University of Technology vol. 126, Gdańsk, Poland, 2012
26. Sabik A, Kreja I. Large thermo-elastic displacement and stability FEM analysis of multilayered plates and shells. Thin Wall Struct 2013;71:119-133.
27. Feng YT., Perić D, Owen DRJ. Determination of travel directions in path-following methods. Math and Comput Modelling 1995;21:43-59.
28. Feng YT, Perić D, Owen DRJ. A new criterion for determination of initial loading parameter in arc-length methods, Comput Struct 1996;58:479-485.
29. de Souza Neto EA, Feng YT. On the determination of the path direction for arc-length methods in the presence of bifurcations and `snap-backs'. Comput Methods Appl Mech Engrg 1999; 179:81-89.
30. Hong T, Teng JG. Imperfection sensitivity and postbuckling analysis of elastic shells of revolution. Thin Wall Struct 2008;46:1338-1350.
31. Sabik A, Kreja I. Imperfection sensitivity of multilayered composite shells. In: Pietraszkiewicz W, Kreja I, editor. Shell Structures: Theory and Applications Vol. 2. London: CRC Press/Balkema, 2010. p 137-140.
32. Chróścielewski J, Makowski J, Stumpf H. Finite element analysis of smooth, folded and multi-shell structures. Comp Methods Appl M 1997;141:1-46.
33. Kreja I. A literature review on computational models for laminated composite and sandwich panels. Cent Eur J Eng 2011;1:59-80.
34. Altenbach H, Meenen J. Single layer modelling and effective stiffness estimations of laminated plates. In: Modern trends in composite laminates mechanics, ICMS 448. Wien New York: Springer Verlag, 2003. p 1-68.
35. Whitney J. Shear correction factors for orthotropic laminates under static load, ASME J Appl Mech 1973;40:302-303.
36. Owen DRJ, Figueiras JA. Anisotropic elasto-plastic finite element analysis of thick and thin plates and shells, Int J Num Meth Eng 1983;19:541-566.
37. Sabik A, Kreja I. The analysis of multilayered laminated plates with the use of equivalent single layer models. (in Polish) Acta Mechanica et Automatica 2008;2:63-68.
38. Ramm E. The Riks/Wempner approach - an extension of the displacement control method in nonlinear analyses. Recent Advances in Non-linear Computational Mechanics. Swansea: Pineridge Press Ltd, 1982. p. 62-86.
39. Kreja I, Schmidt R. Large rotations in first-order shear deformation FE analysis of laminated shells. Int J Nonlinear Mech 2006;41:101-123.
40. Noor AK, Peters JM, Burton WS. Three-dimensional solutions for initially stressed structural sandwiches. J Eng Mech 1994;120:284-303.

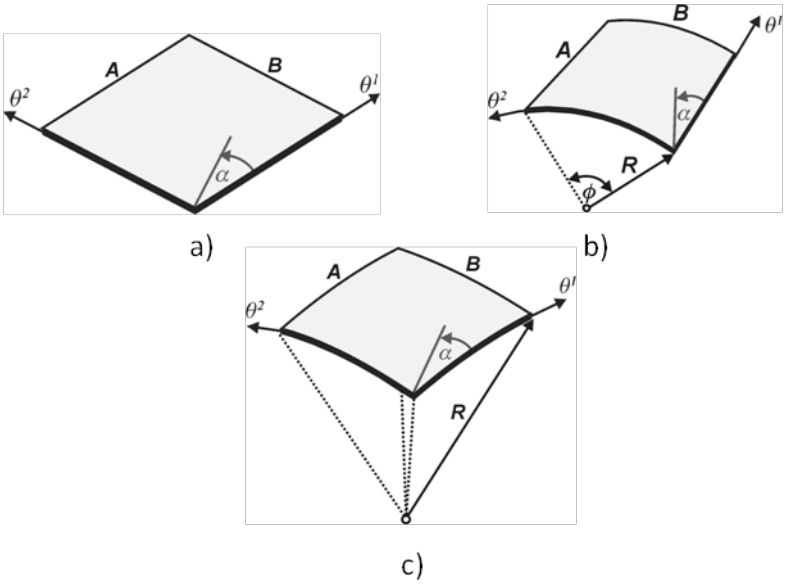

Fig. 1. Geometry of the analyzed panels: a) plate strip, b) plate, c) cylinder, d) sphere

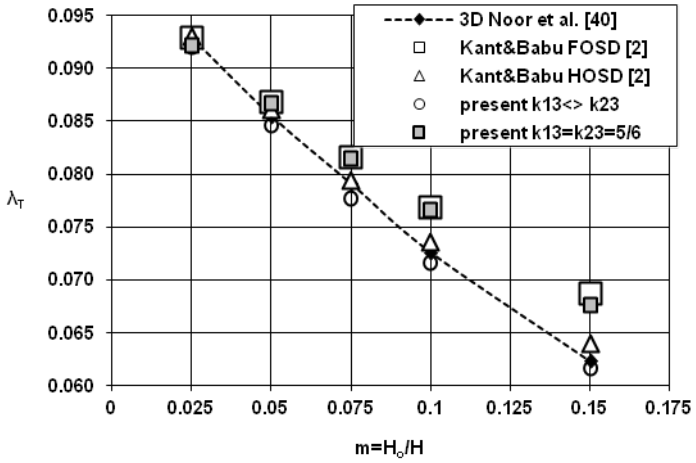

Fig. 2. Sandwich plates, normalized critical temperature λ_T vs. parameter m

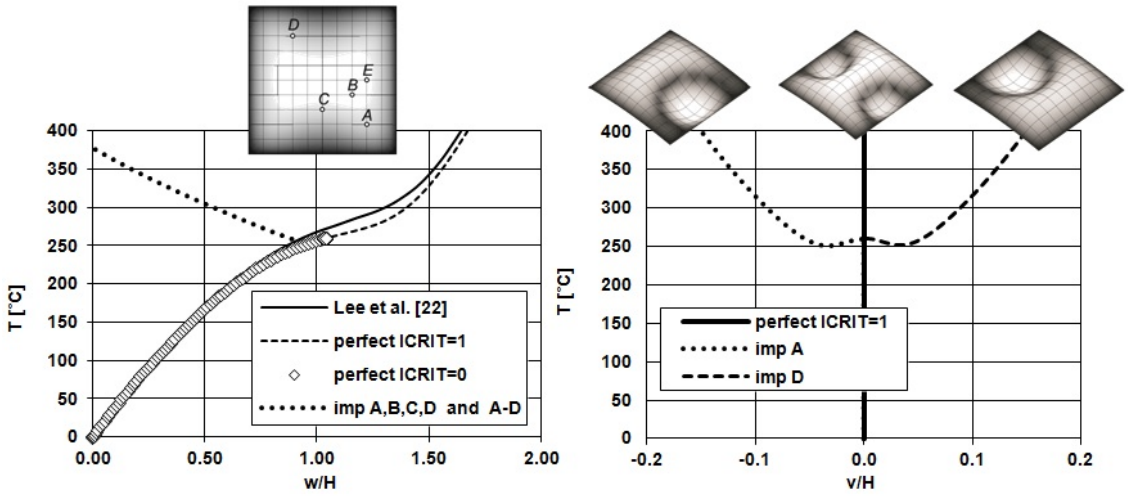

Fig. 3. Cylindrical cross-ply shell: a) normalized central deflection and locations of perturbation forces; b) equilibrium paths of the normalized central circumferential translation

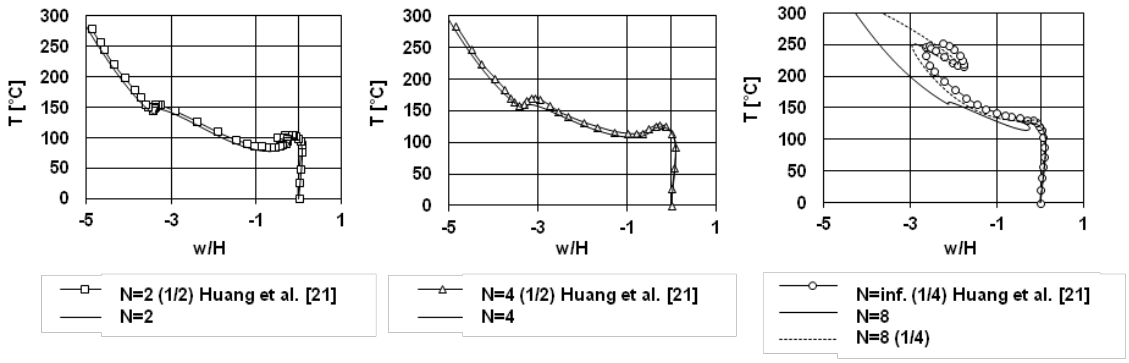

Fig. 4. Cylindrical angle-ply shell, N=2, N=4 equilibrium path of the normalized deflection of the point (A/4; B/3); N=8=∞, equilibrium path of the normalized deflection of the point (7A/24; B/2)

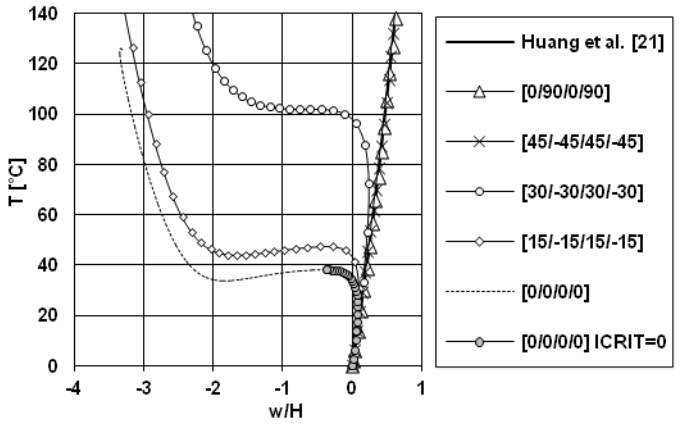

Fig. 5. Spherical shell, the equilibrium paths of the normalized central deflections